International Journal of Rock Mechanics & Mining Sciences xxx (xxxx) xxx–xxx

Contents lists available at ScienceDirect

International Journal of Rock Mechanics & Mining Sciences

journal homepage: www.elsevier.com/locate/ijrmms

Excavation-induced microseismicity in the columnar jointed basalt of an underground hydropower station

Ya-Xun Xiao[a], Xia-Ting Feng[a,*], Bing-Rui Chen[a], Guang-Liang Feng[a], Zhi-Bin Yao[b], Lian-Xing Hu[c]

[a] State Key Laboratory of Geomechanics and Geotechnical Engineering, Institute of Rock and Soil Mechanics, Chinese Academy of Sciences, Wuhan 430071, China
[b] Key Laboratory of Ministry of Education for Safe Mining of Deep Metal Mines, Northeastern University, Shenyang 110004, China
[c] China Three Gorges Corporation, Beijing 10038, China

ARTICLE INFO

Keywords:
Rock mechanics
Columnar joint basalt
Microseismicity
Tunnel excavation
Baihetan hydropower station

ABSTRACT

Large-scale columnar jointed basalt (CJB) developments have had serious adverse effects on the stability of the project in progress to create the diversion tunnels at the Baihetan hydropower station in China. An *in situ* microseismic (MS) monitoring experiment was carried out to help understand the fracturing process in the CJB rock mass as a result of tunnel excavation. MS monitoring performance (accuracy of location estimation and system sensitivity) is analyzed first. Then, the spatiotemporal evolution of the MS activity associated with the Baihetan CJB rock mass fractures along the tunnel axis and at the tunnel sidewalls during the entire excavation unloading process is obtained. Finally, the forms and opportunities to deploy appropriate support are suggested according to the characteristics of the CJB microseismicity. Meanwhile, the MS monitoring methods required for CJB or jointed hard rock engineering (e.g. sensor types, sensor spacing, sensor array forms, system protection, and selection of analysis regions) resulting from this exploration experiment are summarized.

1. Introduction

Understanding and investigating the mechanical behavior of columnar jointed basalt (CJB) has become an important issue in recent years due to its association with engineering production projects. Indeed, its unfavorable rock mechanics have been exposed during several construction processes involving large hydropower and highway projects.[1,2]

Columnar joints are unique geological structures that develop in basalt rocks. They have a primary tensile fracture structure with a regular columnar form. The exploration of their origin and mechanism of formation can be traced back to the 19th century.[3] It is widely accepted that constitutional supercooling plays a major role in the formation of these basalt columns.[4–6] The presence of CJB has been found to have an adverse effect on project stability. During excavation processes in underground caverns with CJB rock masses, serious engineering disasters in the form of major collapses that can cause serious numbers of casualties, mechanical damage, delays to projects, and economic losses have been found to occur. As an example, several intense collapses occurred in 2013 during the construction of the diversion tunnels of the Baihetan hydropower station in China, which have been ascribed to the development of CJB rock masses. The collapses caused the destruction of some large pieces of machinery and equipment, as well as an approximately month-long delay to construction. Therefore, studying the deformation and rules governing the fracture of CJB rock masses in response to excavation is essential, and the results constitute important references for determining construction schemes and identifying support measures.

Obvious differences in deformability and strength have been observed in directions normal and parallel to the axis of a CJB block through a variety of *in situ* observation techniques, e.g. elastic moduli tests, P-wave velocity measurements, and point load determination.[2,7,8] The anisotropic character of the Baihetan CJB arises from its pattern of multi-scale joints and can be explained by means of Goodman's stiffness equation. Based on a theoretical analysis of the rock-quality designation and a representative volume element, Zhang et al. pointed that size effects differ in different directions.[9] Large-scale triaxial compression tests on a CJB rock mass in Hanford, USA indicate that anisotropic deformation in the horizontal and vertical directions decrease distinctly with increasing confining pressure.[10,11] This implies that the anisotropy degree of CJB rock mass increases immensely as a result of excavation.

* Corresponding author.
E-mail addresses: xtfeng@whrsm.ac.cn, xia.ting.feng@gmail.com (X.-T. Feng).

http://dx.doi.org/10.1016/j.ijrmms.2017.04.012
Received 21 June 2016; Received in revised form 18 March 2017; Accepted 22 April 2017

Difficulties with sampling and making rock specimens limit the performance of experimental laboratory studies. Liu et al. carried out a series of physical model tests using a brittle material and truly triaxial apparatus. They found that the stress ratio has a significant effect on the strength, deformation, and failure mode of compound CJB.[12] Scanning electron microscopy of the failure surfaces of the Baihetan CJB rock mass induced by tunnel excavation indicates tensile fracture inside the columns – however, tensile and shear fractures are observed between the columns.[13]

Based on generalized, three-dimensional discrete-element models of the geological structure of CJB rock mass, the representative element volume, strength features, and size effects have also been studied using numerical simulations.[1,14] Although the deformation characteristics and mechanical properties of CJB are understood fairly well, studies on the evolution of CJB fractures during the complete excavation process are extremely rare.

The evolution of disasters resulting from rock engineering activity (such as splitting, rockburst, stress-induced collapse, water inrush, and landside) can, in essence, be seen as a series of rock mass fracture events related to microseismic (MS) events.[15–17] Therefore, *in situ* MS monitoring of rock mass fracture processes has been widely used in rock mechanic testing and rock engineering projects throughout the world.[18–24] Unfortunately, most MS signals related to CJB fracture are of low amplitude, have high frequency, and are seriously attenuated. However, an exploratory test at the 4# diversion tunnel of the Baihetan hydropower station (Region B shown in Fig. 1b) indicated that MS technology can be used to observe the fracturing process in the CJB rock mass during tunnel excavation.[25] Unluckily, that particular experiment had to stop due to a failure of the communication units when most of the monitoring region was still unexcavated. Thus, the anticipated research covering the whole of the fracture process in CJB under tunnel excavation was not finally realized. Therefore, the following important questions still need to be answered: (i) How should we best carry out MS monitoring in rock projects involving CJB developments or jointed hard rock? (ii) How does CJB rock mass fracturing respond to excavation unloading? (iii) How do we use the results from MS monitoring to guide the construction of CJB engineering projects?

This paper focuses on the three abovementioned key issues and summarizes the results from MS monitoring experiments carried out as part of an *in situ* observation experiment on the CJB tunnel at the Baihetan hydropower station in Sichuan, China. The Baihetan diversion tunnels are the first tunnels engineered in a large-scale CJB development.

2. *In situ* microseismic experiments on the CJB tunnel

2.1. Field description

The Baihetan hydropower station is located on the border between Ningnan County, Sichuan and Qiaojia County, Yunnan. It is the second cascade of four hydropower stations in the lower reaches of the Jinsha River, as shown in Fig. 1a. The station, with a total capacity of 2.06×10^{10} m^3 and an installed capacity of 16000 MW, will function as a significant multipurpose water conservancy project, similar to the Three Gorges hydropower station. A river closure and tunnel diversion technique is being adopted in the construction process. Accordingly, diversion tunnels (three on the left bank and two on the right) are located along the direction of water flow. The dam area of the Baihetan hydropower station is mainly composed of Upper Permian Emeishan Formation basalt with 11 rock layers ($P_2\beta^1$– $P_2\beta^{11}$). The CJB rock masses occur mainly in the $P_2\beta_3^2$ rock layer. There are lengths of about 440–560 m which have CJB rock mass developments in each of the five diversion tunnels. The locations of the diversion tunnels and the

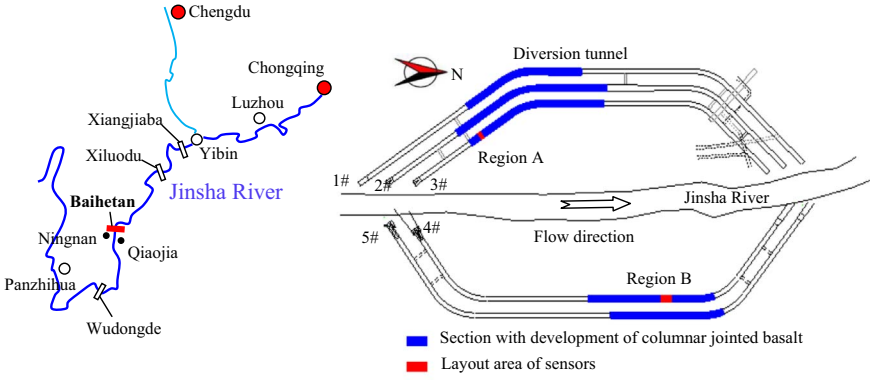

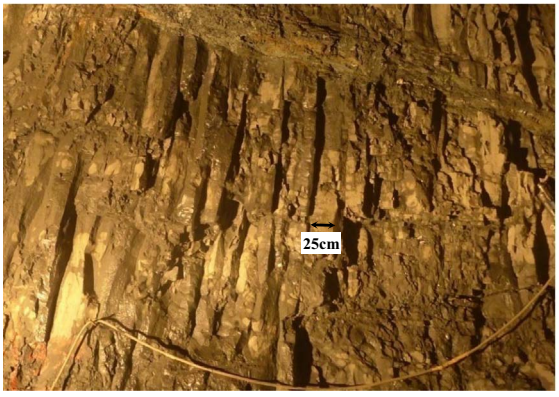

(c)

Fig. 1. Background information on the MS monitoring project: (a) geographic location of the Baihetan hydropower station, (b) arrangement of the five diversion tunnels and the distribution of the CJB, and (c) CJB rock masses exposed in the MS monitoring region.

distribution of the CJB are shown in Fig. 1b.

The 3# diversion tunnel, which is close to the bank of the Jinsha River, has a total length of 1586.9 m and is parallel to the adjacent 2# diversion tunnel (the tunnel spacing is 60 m). According to the stratum exposed during tunnel excavation, this tunnel coincides with monoclinal strata with a strike of 40°N–50°E, SE tendency, and a dip of 15–25°. The lithology of the surrounding rock mass is mainly aphanitic basalt, amygdaloidal basalt, and tuff in four rock layers (i.e. $P_2\beta_2^3$, $P_2\beta_3$, $P_2\beta_4^1$, and $P_2\beta_4^2$).

For this MS monitoring experiment, the section K0+310–K0+325 of 3# diversion tunnel was selected for sensor deployment (Region A in Fig. 1b). According to the geological conditions exposed during upper excavation, the experimental region belongs to the $P_2\beta_2^3$ rock layer and has developed CJB rock masses with column diameters of 5–25 cm (see Fig. 1c). There no macroscopic geological structures, such as faults and bedding fault zones. The hydrogeological aspect is dry without water. Laboratory rock tests indicate that the density of the rock blocks in the CJB is about 2.90 g/cm^3 and that the average uniaxial compressive strength and deformation modulus are 100 MPa and 65.1 GPa, respectively.[7] *In situ* stress measurements show that the maximum major principal stress in the experimental region reaches 22.0 MPa and is approximately horizontal, which is classified as a moderate to high stress level.[26]

2.2. Microseismic monitoring scheme

Four important lessons were learned from the previous MS tests in the 4# diversion tunnel: (i) accelerometers with high sensitivity and frequency should be selected; (ii) the testing areas should be selected on the same side of the diversion tunnel; (iii) the distance between the sensors in adjacent rows should be reduced (compared to that used previously); and (iv) protection of the communication lines and sensor installation areas should be given serious consideration. A comparison of the main parameters of the MS systems used in the 3# and 4# diversion tunnels are listed in Table 1. A detailed description of the new MS experiments carried out in 3# diversion tunnel is as follows.

The experimental tunnel (typically 20 m wide and 24 m high in the transverse section) was excavated from the upper, to middle, to lower layers with excavation heights of 8, 10, and 6 m, respectively, as shown in Fig. 2. The upper layer had been excavated before this MS experiment began. The MS monitoring system was built based on an integrated seismic system (ISS). The hardware composition of ISS has been introduced in Ref. 25 and its software for MS data processing and results presenting can be got from http://www.imseismology.org/. The whole monitoring system can be divided into three parts: the sensor array, communication lines, and monitoring center (see Fig. 2a). The sensor array was composed of six uniaxial and two triaxial accelerometers. The sensitivity of these accelerometers was 1 V/g and the approximate usable frequency response varied from 0.5 to 8000 Hz. Four monitoring sections, each consisting of two accelerometers, were arranged at intervals of 5 m from the chainage 0+310 to 0+325. The MS sensors were embedded using the space presented by the upper excavation. The locations and types of these sensors are shown in Fig. 2b and c. The communication lines (in lengths of 170–200 m) consisted of twisted-pair cables made from copper conductors (20 American wire gauge) and shielded with aluminum coils. The monitoring center mainly consisted of the center server and two 6-channel MS data acquisition units. The equipment in the monitoring center was safe throughout the entire monitoring program as it was located at an interconnection between the 2# and 3# diversion tunnels.

The previous MS testing in 4# diversion tunnel performed in 2012 was interrupted when serious damage occurred to the communication cables as a result of blasting. The monitoring conditions in the 3# diversion tunnel were similar to those in the 4# diversion tunnel. This suggested that two parts of the MS monitoring system (the sensor array and communication lines) were at serious risk of being destroyed. Therefore, a protection scheme was proposed and implemented to prevent any damage occurring and to safeguard the continuity of the collected data. The safeguard procedure involved the following steps: (i) In the region used for sensor installation, several grooves with approximate depths of 10 cm were cut using a pneumatic drill (Fig. 3a). Then, the cables and junction boxes of the sensors were put inside these grooves and the grooves manually filled with cement grout. Wooden boxes were subsequently added to the surfaces of the aforementioned protected areas (Fig. 3b). (ii) As shown in Fig. 3c, the communication lines were first mounted onto the sidewall of 3# diversion tunnel (2 m off the ground, in the upper layer). They passed through U-shaped steel conduits each of length 50–100 cm. (iii) Reinforced steel fiber concrete was finally used to cover (to a thickness of 20 cm) the entire sensor array and communicate lines, and this formed a part of the system support for the upper excavation area (Fig. 3d). We note that the cables could not be directly covered with the reinforced concrete because the steel fibers used could have cut the cables when subjected to the high-pressure grouting process. It took us 20 days to complete all of these protection measures, but the effort involved proved to be worthwhile and very valuable results were subsequently obtained.

2.3. Excavation information and implementation of the microseismic experiments

A construction access tunnel at chainage 0+260 to 0+275 was excavated from the adjacent 2# diversion tunnel to speed up the excavation progress in the test tunnel. Then, excavation of the middle layer of the test tunnel started on 23 March 2013 by making use of this construction access. The excavation process followed a traditional drilling and blasting format (the blasting process used was identical to that used in the 4# diversion tunnel). Details of the blasting process and parameters involved can be found in a related paper.[24]

The length of each excavation round was 10 m in the direction of the tunnel heading. When the tunnel face had advanced to chainage 0+380 (on 13 May 2013), excavation of the lower layer began (at chainage 0+270). The position of the tunnel face relative to the sensor array center as a function of time is shown in Fig. 4. Tunnel support was deployed in the middle layer at this site including: mortar bolts (28 mm diameter, 6 m long, and spaced at 1.2 m×1.2 m), and reinforced steel fiber concrete (to a thickness of 15 cm). In addition, the excavation region is not supported immediately. These supports were implemented far away from tunnel face 30–60 m.

Table 1
The main analysis parameters for the MS systems employed.

Diversion tunnel	Year	Sensor information				Sensor array	
		Type	Quantity	Bandwidth (Hz)	Sensitivity	Row spacing (m)	Location
3#	2013	Uniaxial accelerometer	6	0.5–8000	1 V/g	5	One side of tunnel
		Triaxial accelerometer	2				
4#	2012	Uniaxial geophone	6	7–2000	80 V/m/s	15	Both sides of tunnel
		Uniaxial accelerometer	2	0.5–8000	1 V/g		

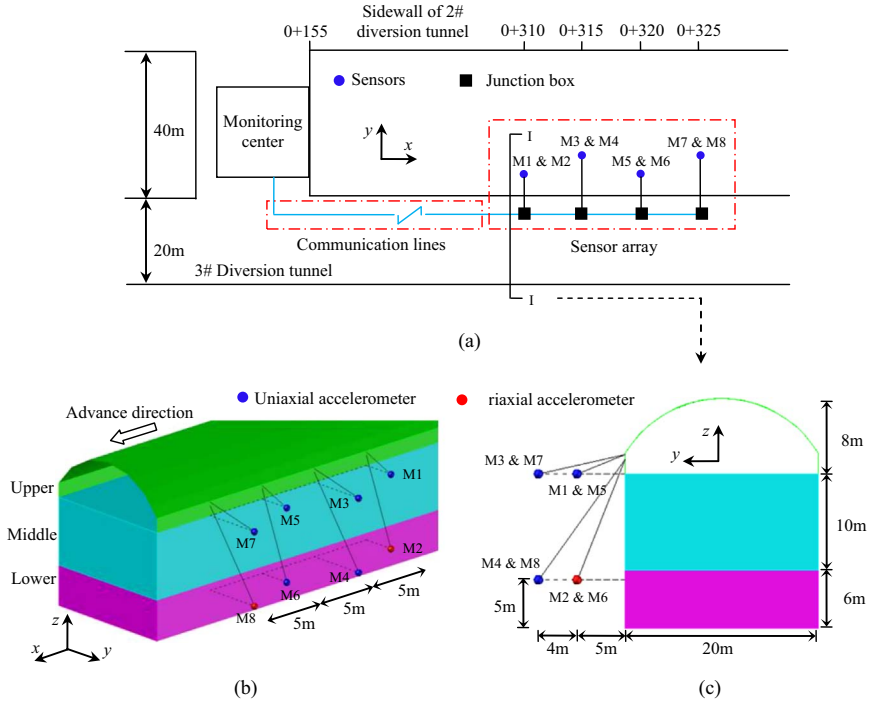

Fig. 2. Layout of the microseismic monitoring system: (a) overall layout, (b) a three-dimensional representation of the sensor array layout, and (c) a two-dimensional cross-section of the tunnel.

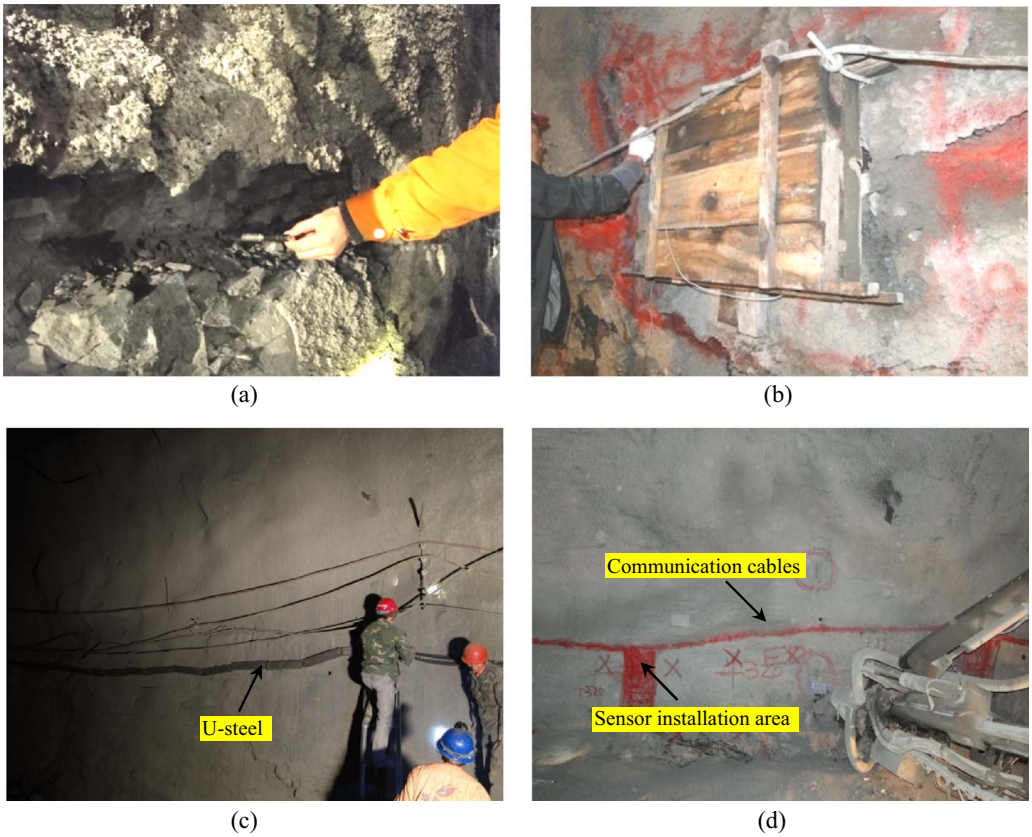

Fig. 3. The procedure used to safeguard the microseismic monitoring system: (a) grooves cut to protect the array, (b) wooden boxes covering the sensor array, (c) U-shaped steel conduits for fixing the communication lines, and (d) final covering with reinforced steel fiber concrete (to a thickness of 20 cm).

The MS monitoring system was completed on 23 February 2013. Monitoring of the excavation of the abovementioned construction access was used to pre-test the system for debugging purposes. The official MS experiment began on 23 March 2013 when the middle layer of the test tunnel was being excavated. Our research focused on the fracturing process in the CJB rock masses due to excavation of the middle layer. According to the excavation process of the test tunnel, the period from 23 March to 13 May was selected to use for analysis

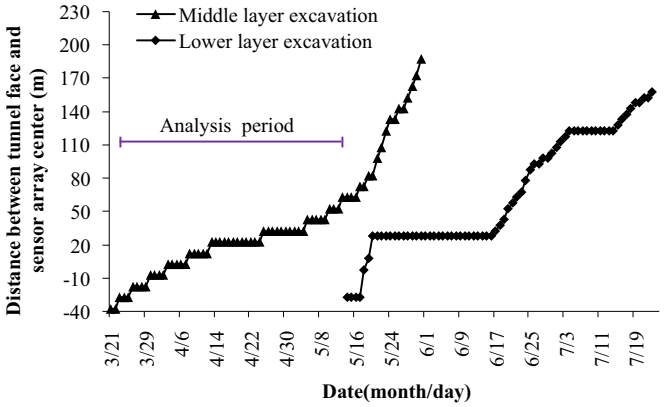

Fig. 4. The excavation process in the test tunnel.

(Fig. 4). At the beginning and end of this period, the center of the sensor array was about twice the tunnel diameter prior to, and thrice the tunnel diameter posterior to, the tunnel face, respectively.

3. Monitoring performance

3.1. Location accuracy estimation

Analyzing location accuracy is a fundamental aspect of interpreting the MS results. A constant velocity model is assumed here for MS-source location purposes. That is, the velocities of the elastic waves (P- or S-) are taken to be the same in all directions. In order to achieve a more precise MS source location, three or four instantaneous 'small dosage' blasts (charges of 2–3 kg) were detonated every two excavation cycles to invert the propagation velocities of the P- and S- waves. According to the co-ordinates and arrival times at the trigger sensors and the co-ordinates and times of the blasting events, a series of velocities for the elastic waves (P- and S-) could be estimated using the following expression:

$$\Delta t_k = t_{k+1,P,S} - t_{k,P,S} = \frac{L_{k+1} - L_k}{v_{P,S}} = \frac{\Delta L_k}{v_{P,S}} \quad (1)$$

where $t_{k,P,S}$ is the arrival time of the P- or S-wave at the k-th sensor, $v_{P,S}$ is the velocity of the P- or S-wave, and L_k is the blast–sensor distance. The latter can be expressed as follows:

$$L_k = \sqrt{(x_k - x)^2 + (y_k - y)^2 + (z_k - z)^2}, \quad (2)$$

where (x_k,y_k,z_k) corresponds to the position co-ordinates of the k-th sensor, and (x, y, z) to the position of the fixed blast point.

The velocities used in our source location work correspond to the mean values of these calculated velocities. Taking the calibrated blast signals on 4 April 2013 as an example, the velocity model was identified based on the method mentioned above, and the result indicated that $v_P = 5470.8$ and $v_S = 3500.2$ m/s.

The C-optimality method[27] was used to design an optimal sensor array to estimate the location accuracy in the monitoring area. The main parameters in the analysis are listed in Table 2. As the location errors caused by the location algorithm were not considered, some parameters were set to values greater than their real ones (i.e. wave velocity errors, site measurements, and arrival times). In Table 2, 'PPV' refers to the 'peak particle velocity' at the sensor site.

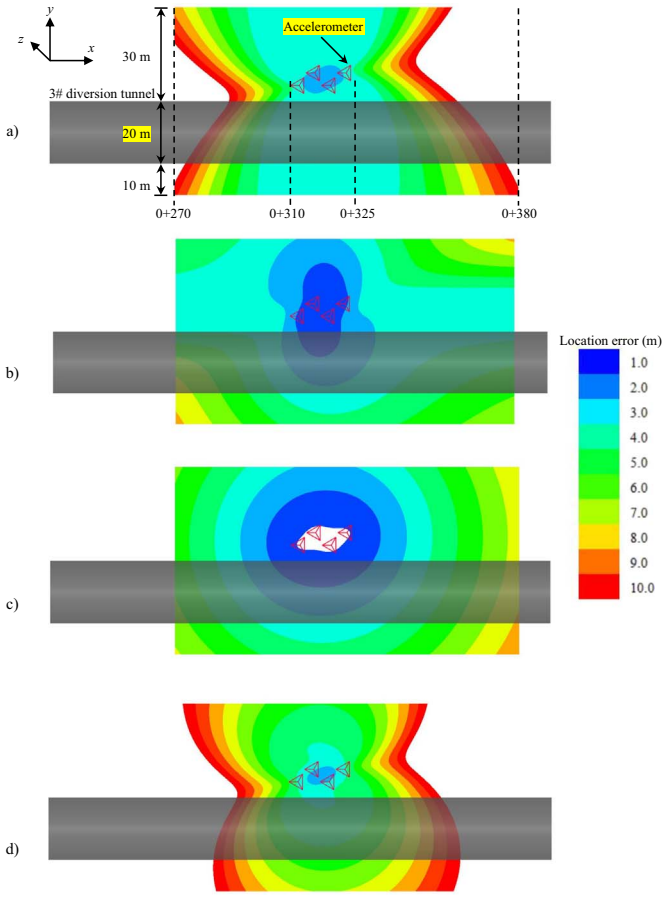

Fig. 5. Estimation of the location accuracy showing the errors along the: (a) x, (b) y, and (c) z directions. (d) The spatial location error. The directions of x, y, and z are defined to be along the tunnel axis, pointing into the left sidewall, and vertically upwards, respectively.

The MS sources analyzed here were located on the center plane of the middle layer of the test tunnel (tending towards the tunnel side with the sensor array). Isograms of the location errors in different directions and for the whole system were drawn accordingly (Fig. 5). Overall, as the figure shows, location of the MS source in most of the monitoring area involved an error of less than 10 m, which is perfectly adequate. The further the MS source is away from the sensor array, the lower the location accuracy. The location error along the direction of the tunnel axis makes the key contribution to the total error, as it is much bigger than in the other two directions. It is therefore better to choose an analysis region around the sensor array to reflect the microseismicity of the CJB fracturing process along the tunnel axis. In contrast, the high location accuracy on the tunnel section (which can be less than 1 m) effectively ensures the reliability of MS activity at the sidewall where the sensor array is located.

3.2. System sensitivity

'System sensitivity' refers to the smallest magnitude MS event that

Table 2
Main parameters used to estimate location accuracy. (Note: a constant velocity model is used.).

Parameter:	Velocity parameters (m/s)			Site measurement error	Minimum number of trigger sensors	Minimum PPV that sensor can resolve (m/s)	Pick error	
	P-wave	S-wave	Error				P-wave (s)	S-wave (s)
Value:	5460	3430	10%	2%	5	2.0×10^{-5}	0.0006	0.0015

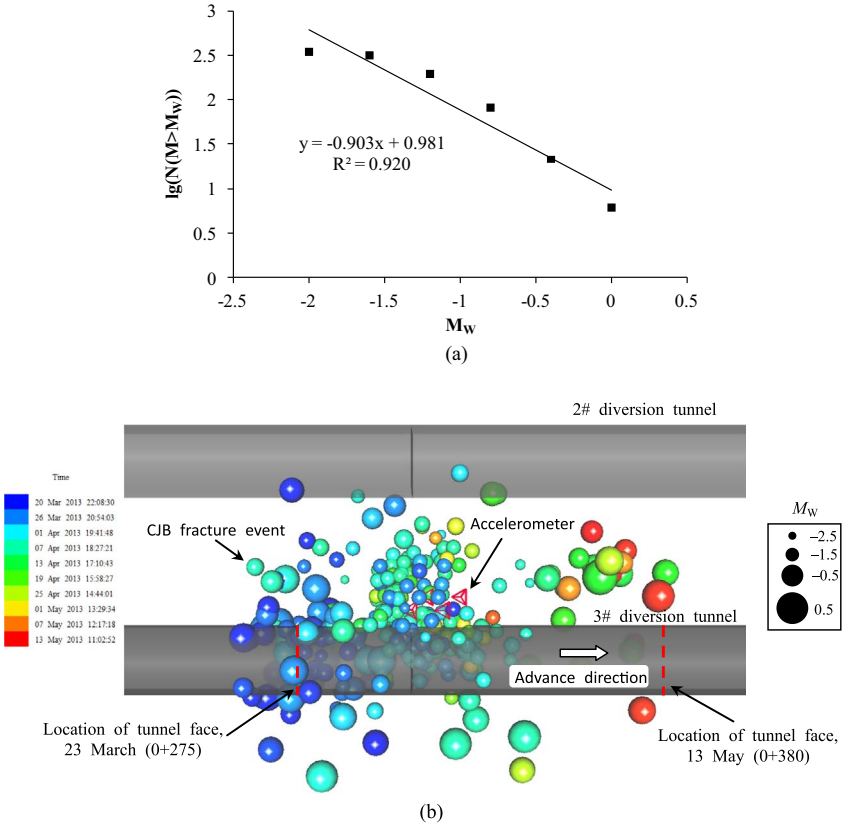

Fig. 6. The CJB fracture events monitored during the analysis period, showing: (a) b-value of M_W, and (b) their spatial distribution. N means the number of events with M_W bigger than the specific value.

can be monitored by the MS system (the smaller the magnitude that can be monitored, the greater the system sensitivity). During the analysis period, 360 MS events due to CJB fracture were recorded. Using the method devised by Hanks and Kanamori,[28] a 'moment magnitude', M_W, can be calculated to characterize the size of a CJB fracture in terms of the amount of seismic moment. The distribution of the moment magnitudes associated with these events is shown in Fig. 6. The minimum M_W value that could be monitored reached −2.3. Also, over 92% of the CJB fracture events registered M_W values in the range −2.0 to −0.4. This implies that the most of the CJB fracture-induced MS sources resulting from excavation unloading radiated low MS energies and that the scale of these fractures was small. The relation between CJB microseismicity and its Mw is shown in Fig. 6a. It can be seen that a believable b-value can be got. During excavation of the monitored CJB region, the characteristics of the rock mass fractures in the different zones should be almost the same due to their similar mechanical properties (type of rock mass, geological condition, excavation parameters, and support used). However, the frequency and spatial distributions of the moment magnitudes associated with these events are very distinct in different zones (Fig. 6b). In Fig. 6b, each sphere represents a CJB fracture event. The colors and sizes of the spheres represent the times and moment magnitudes of those events, respectively.

The M_W values of the events can be further analyzed along the direction of the tunnel axis to help explain this phenomenon (Fig. 7). The maximum M_W values are roughly equal for events in the different statistical zones with lengths of 10 m. However, the minimum values decreased quickly with increasing distance to the sensor array center (in the direction of the tunnel axis). This is why the further away from the sensor array you are, the fewer the number of CJB fracture events are recorded (Fig. 6b). The obvious difference in the microseismicity between statistical zones is caused by the variation in the monitoring sensitivity in each zone. Therefore, the variation in the monitoring

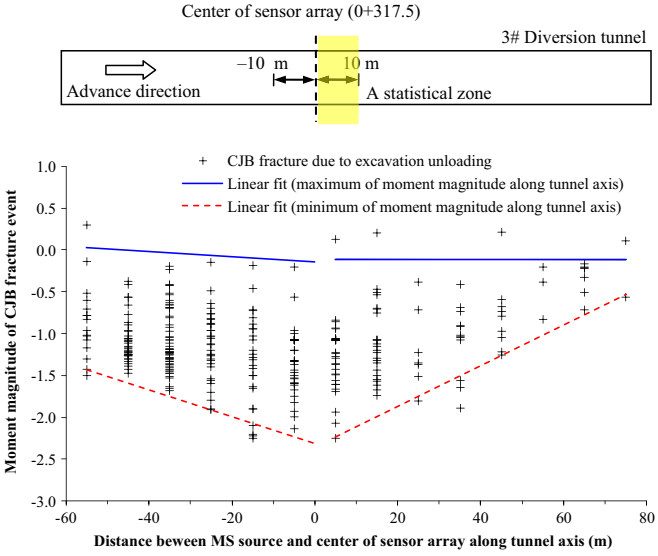

Fig. 7. The distribution of the moment magnitudes associated with CJB fracture events along the tunnel axis.

sensitivity was studied further in order to determine the analysis region for CJB microseismicity.

The relationship between the maximum distance between MS source and triggered sensor (D_{max}) and moment magnitude is shown in Fig. 8. As can be seen, the relation between the maximum in D_{max} increases linearly as the moment magnitude of the CJB fracture event increases. The monitoring sensitivity in the different zones drops quickly away from the sensor array, as is clearly illustrated in Fig. 8b. The strong attenuation of the CJB fracture signal is the reason behind this monitoring result.[25] Fig. 8 may be used as a useful guide for

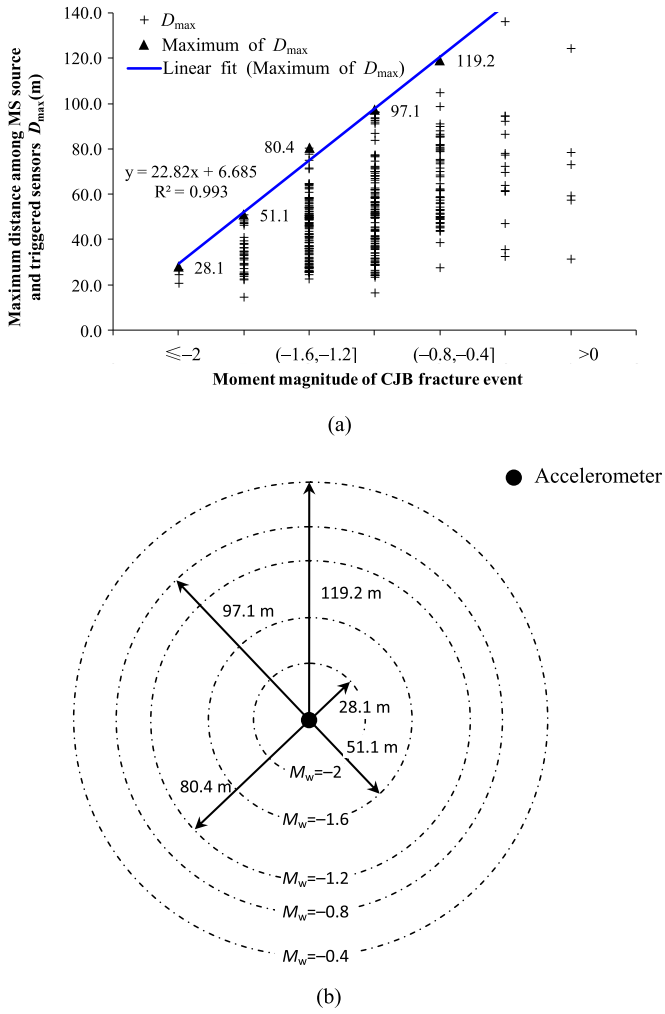

Fig. 8. MS system sensitivity in the CJB tunnel: (a) the relationship between the hypocentral distances of the trigger sensors and the moment magnitudes of the CJB fracture events, (b) sensitivity contours for the accelerometer.

similar MS monitoring activities in jointed rock engineering in the future. For example, if the expected monitoring sensitivity for a specific region (i.e. the minimum detectable moment magnitude of a CJB fracture event) was −1.6, then the maximum distance between triggered accelerometers and this region corresponds to 51.5 m. The number of triggered accelerometers should be chosen to satisfy the demand of the event location.

An additional and interesting result is that the CJB fracture events on the opposite side from where the sensor array is located are difficult to capture and observe. The reason behind this is that the excavated volume (i.e. region where excavation has already taken place) has a significant effect on preventing the propagation of the MS wave radiated from the CJB fracture source. Therefore, the daily CJB fracture event count at the left-hand sidewall of the tunnel was much less than that at the right-hand side. It also decreased quickly as the excavated volume expanded due to the excavation of the middle layer of the test tunnel (Fig. 6b).

4. Results

4.1. Selection of analysis region

The analysis region, which needs to be selected *before* beginning work, can be determined according to the following three requirements[1]: The monitored MS information in the analysis region has to reflect the complete time-evolution process of the CJB microseismicity caused by tunnel excavation.[2] High location accuracy in the horizontal plane is required to precisely represent the spatial evolution in CJB microseismicity.[3] High, and uniform, monitoring sensitivity is required to ensure the representativeness and reliability of the monitoring results.

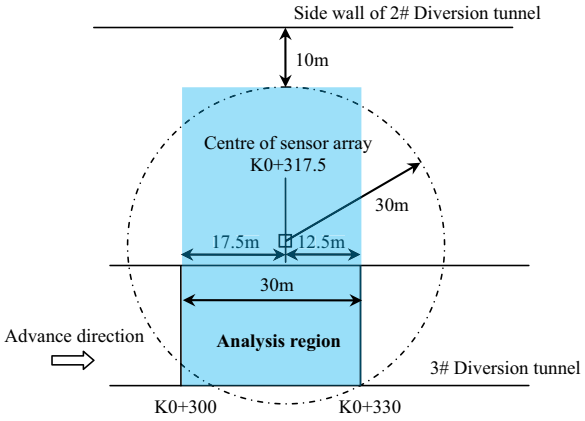

Fig. 9. Selection of the analysis region.

According to these selection principles, the 'best' analysis region is from 0+300 to 0+330 (Fig. 9). In this region, the location errors in each direction were less than 4 m and the monitoring sensitivity could reach −2.0. The results of previous studies indicate that the scope of influence of the tunnel excavation prior to and posterior to the tunnel face is 1–2 times and 2–3 times the tunnel diameter, respectively.[29,30] The distance between the center of the analysis zone and the tunnel face at the start and end of the monitoring experiment is 40 and 65 m, respectively (i.e. about 2 and 3.25 times the tunnel diameter). Therefore, the CJB microseismicity in the analysis region can reflect the whole effect of the excavation unloading process.

4.2. Spatiotemporal evolution along the tunnel axis

Almost 56% of the total recorded MS events (201 events) were located in the analysis region. The relative positions of the CJB fractures with respect to the tunnel face at the time the CJB fracture occurred are shown in Fig. 10. Due to the microseismicity in the whole of the monitored region, the distribution of CJB fractures along the tunnel axis can be divided into three parts: the excavation unloading, mixed effect, and aging relaxation regions. The average event counts per meter in these regions are 6, 2 and 0.6 respectively.[31]

As shown in Fig. 10a, the ranges of the excavation unloading and aging relaxation regions are [−1.6d, 2d] and [−4d, −2.4d], respectively, where d is the tunnel diameter (20 m). CJB fractures in the mixed effect region are caused by the combined influence of excavation unloading and aging relaxation and are located in the interval between the other two regions. The event count along the tunnel axis fits a logistic distribution based on three parameters. The maximum distance of the analysis region from the tunnel face reached 70 m (3.5 times d). A similar distribution to that shown in Fig. 10a should reappear within the analysis region. However, the final results revealed the effects of excavation unloading only (see Fig. 10b). Few events occurred in the regions corresponding to mixed effects and aging relaxation (and especially the latter).

Therefore, we performed a further study of the evolution of the event count *vs*. tunnel excavation and support. The temporal evolution laws observed are shown in Fig. 11. It can be seen that the relative position of the analysis region (with respect to the tunnel face) allowed the CJB microseismicity of the whole process to be determined. MS activity increased step-by-step as the tunnel face approached towards the analysis region (from 23 to 30 March). It then reached its most

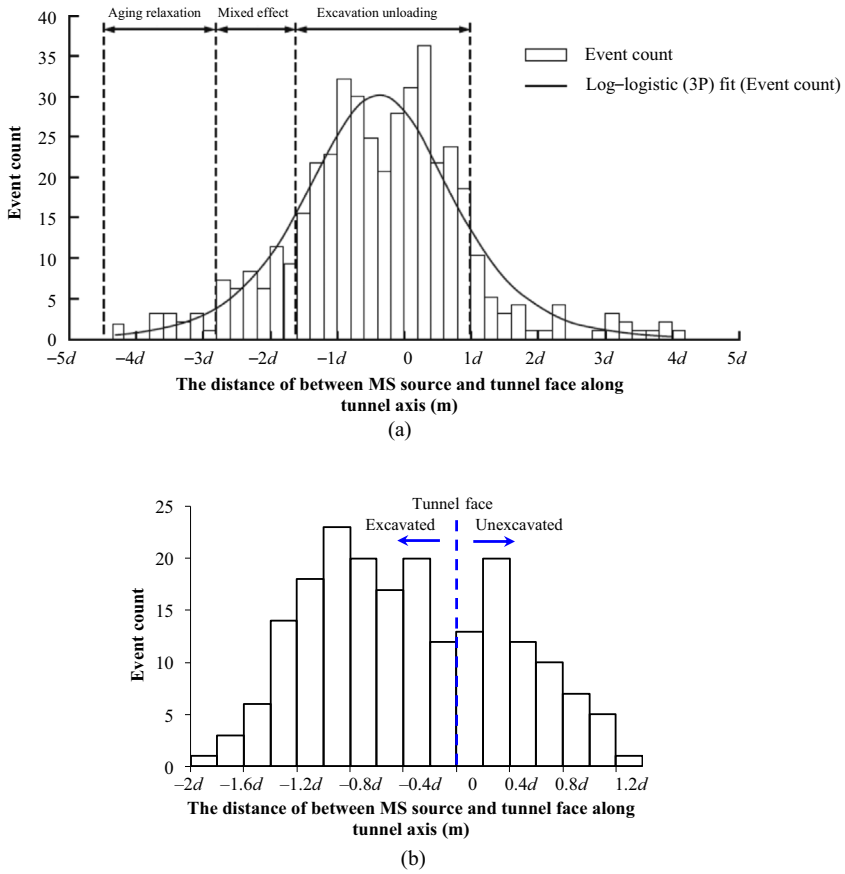

Fig. 10. Distribution of CJB fracture events along the tunnel axis for: (a) the whole of the monitored region (Feng 2015), and (b) the analysis region. The tunnel diameter, *d*, is equal to 20 m.

active level during the excavation of the analysis region. The daily event count reached its maximum value (over the whole excavation process) of 30 on 8 April, after the last blasting event of the excavation cycle in the analysis region. Subsequently, the MS activity decreased quickly as the tunnel face moved further away from the analysis region. As there were only a few occurrences of fracture events after 24 April, the surrounding CJB in the analysis region can be considered to have been in a stable condition from this day onwards. During each excavation cycle, excavation unloading is the major factor controlling CJB fracture activity. Its effects can last nearly 3 days.

The most important piece of new information learned from the monitoring results is that timely introduction of support is able to effectively smother the effects of aging relaxation. MS activity associated with aging relaxation was rare after the support measures were finished in the analysis region (on 25 April).

4.3. Spatiotemporal evolution at the tunnel sidewall

The way in which seismic events evolve at the tunnel sidewall can be illustrated using event-count 'clouds' (Fig. 12). In the analysis region, the process can be divided into three stages corresponding to the features of the microseismicity that are occurring. The stages can be summarized as follows: (i) *Discrete development* 23–30 March): As the tunnel face advance towards the analysis region, MS activity gradually

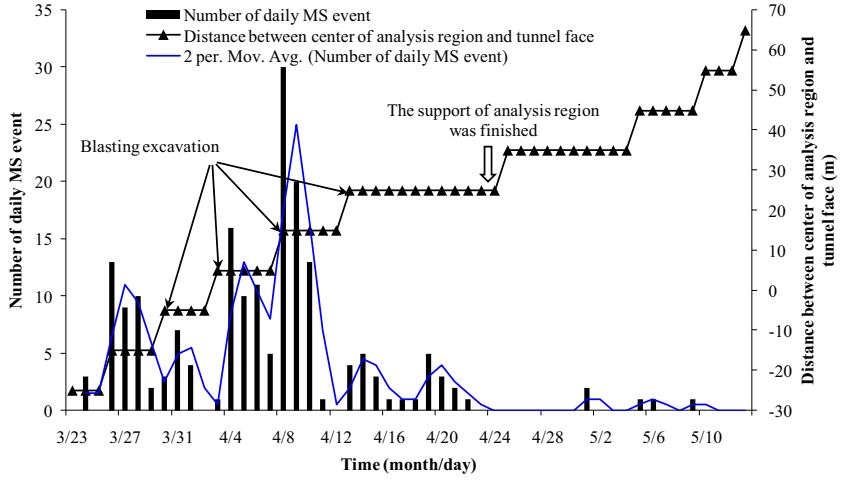

Fig. 11. The temporal evolution of the CJB microseismicity resulting from tunnel excavation and implementation of support measures.

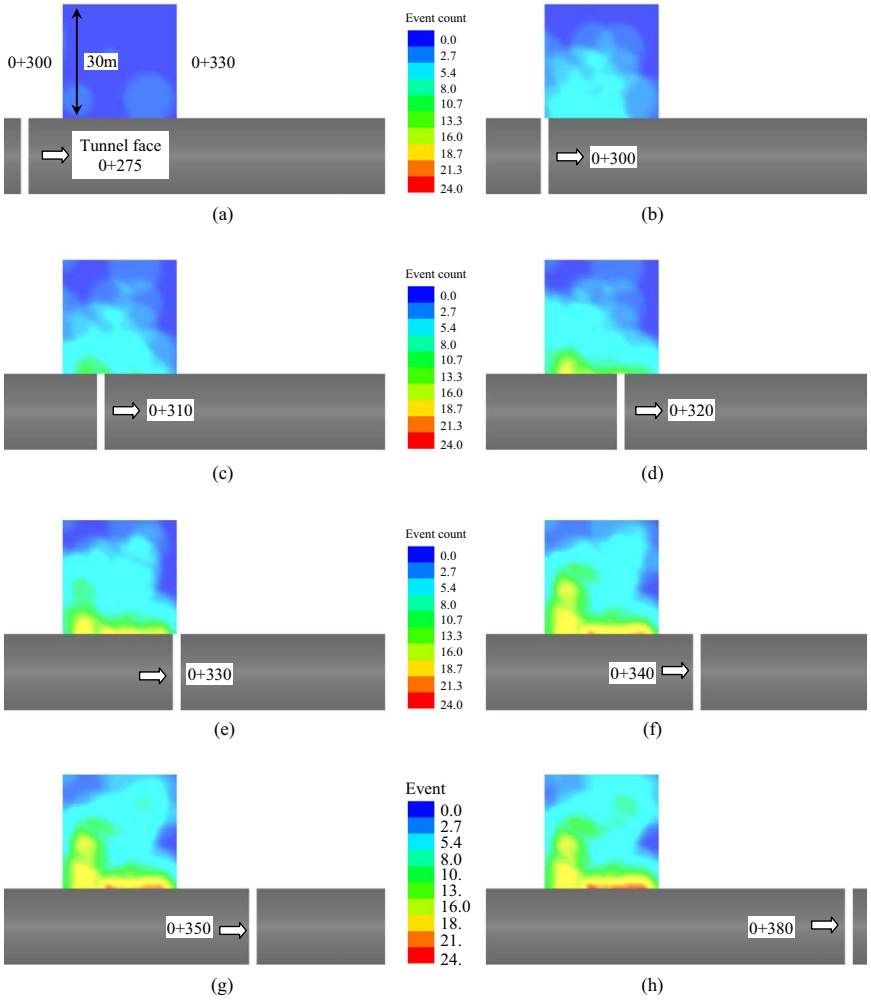

Fig. 12. Evolution of the event count cloud in the analysis region from 23 March to (a) 25 March, (b) 29 March, (c) 2 April, (d) 7 April, (e) 12 April, (f) 24 April, (g) 4 May, and (h) 13 May.

increases. Overall, the MS events are not focused in any particular zone (Fig. 12a and b). (ii) *Fast concentration* (31 March to 24 April): The density of the MS events varies greatly during each excavation cycle. MS activity rapidly becomes more concentrated near the sidewall of the excavated analysis region. Meanwhile, the area within which the fractures are concentrated at the tunnel sidewall constantly develops, from the surface towards the interior. Until the analysis region had been supported, and the tunnel face is moving away from the analysis region (~10 m), the microseismicity distribution is essentially stable (Fig. 12c–f). (iii) *Calming stage* (25 Apr to 13 May): The overall structure of the MS activity in the analysis region does not change any more. Several MS events occur at the surface of the tunnel sidewall (Fig. 12g and h).

Fig. 13 shows with greater clarity the way the MS activity evolves at different depths inside the sidewall. As can be seen, the numbers of CJB fracture events counted in the depth ranges [0,3] and [3,6] (in meters) are several times those occurring in the other ranges. Therefore, the area of concentration of the CJB fractures resulting from tunnel excavation is registered within the range from 0 to 6 m. Paradoxically, the event counts at 15–18 m depth *exceed* those in the ranges 6–9, 9–12, and 12–15 m. The reason for this is a mixed excavation effect in this deeper region associated with the test tunnel and the adjacent tunnel (the middle layer of 2# diversion tunnel had been excavated before the MS experiment was performed).

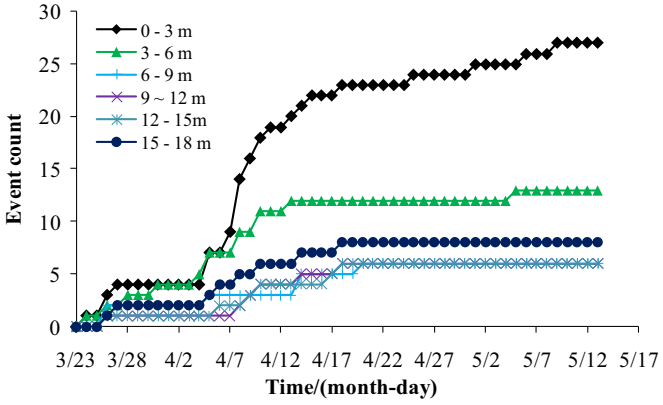

Fig. 13. Temporal evolution of the event count at different depths inside the sidewall.

5. Discussion

An appropriate MS method for monitoring the fracture processes in CJB or jointed hard rock can be summarized as follows. As the radiated energy is small and most of the CJB fracture signals are rapidly attenuated, it is not advisable to perform MS monitoring over a large scale in the construction region. However, *in situ* rock testing in a small, specific region is very important and reliable with the aid of MS technology, and can be used to understand the rock mass fracturing processes associated with engineering production. The MS tests pre-

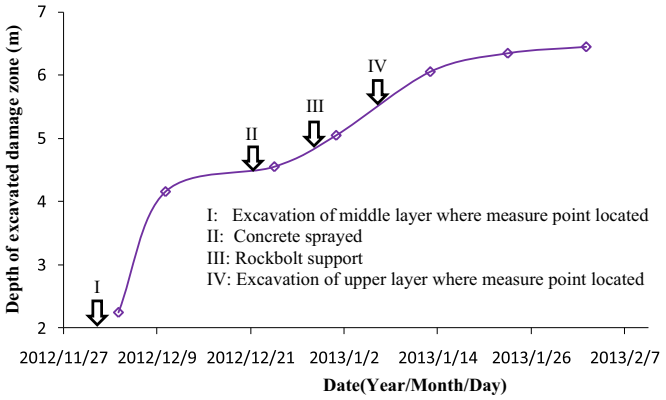

Fig. 14. The typical evolution of the excavated damage zone of a CJB tunnel section as measured via sonic wave tests in a borehole.

sented here are good examples. The basic method for *in situ* MS monitoring of rock mass fracturing processes has been suggested in 32. For CJB, or jointed hard rock, engineering some additional points need to be addressed when carrying out MS monitoring: (i) Accelerometers with high sensitivities and frequencies are better MS sensors than geophones. (ii) The null volume produced during excavation significantly affects the acquisition of CJB fracture signals and must be given serious consideration when designing the sensor array. One solution is to arrange the sensor array on one side of the null volume, as suggested in this paper (see Fig. 2). Another possibility is that the accelerometers could be interactively applied around the null volumes. (iii) The sensor space needs to be set up carefully due to the rapid variation in the monitoring sensitivity. Carrying out pre-tests to determine the monitoring sensitivity relative to the hypocentral distance of the sensor is suggested (as presented in Fig. 8). (iv) As with the arrangement of the MS system presented in this paper, where most of the components were located near to the excavation face (the sensor array and communication cables, etc.), sufficiently strong protection measures need to be implemented. The measures used in this work can be taken as reference (see Fig. 3). (v) The selection of the analysis region needs to satisfy the monitoring purpose and the demands placed on location accuracy and monitoring sensitivity. In addition, the appropriate location method (such as double-difference location method) can be used to improve the location accuracy.

Some lessons can be learned from our MS tests in regard of support measures. Our MS results indicate that supporting the MS analysis region is required to control relaxation fracture of the CJB. The excavated zone needs to be supported timely with shotcrete and rock bolts within the microseismic region of the excavation unloading region (Figs. 10 and 11). In short, the posterior distance from the support to the tunnel face needed to be less than 1.6 times the tunnel diameter in our case. However, it is not recommended to implement support immediately after excavation. Stress redistribution and energy release in the CJB rock mass surrounding the newly excavated region (and the accompanying microseismicity active) is very severe and can last 2–3 days (see Fig. 11). Meanwhile, it is inevitable that there will be large deformations in the surrounding CJB rock mass formed in this period which are difficult to control.[33] Prematurely implemented support could fail at a later date (e.g. the shotcrete may crack, rock bolts break, etc.), and also wastes the opportunity to take advantage of potentially good self-realized stability within the CJB rock mass.

Based on the MS results, some suggestions as to the form of support can also be given. The MS activity is initially mainly concentrated near the sidewall surface, but then gradually develops towards to the interior of the surrounding rock mass (see Fig. 12). The evolution of the excavation damaged zone (EDZ), as measured by sonic wave testing in a borehole (Fig. 14), is in agreement with this pattern of evolution. According to this result, spraying the concrete onto the newly excavated zone as soon as possible after the excavation period is not a suitable method of supporting the tunnel to restrain fracture processes in the CJB rock mass near the sidewall (as already discussed above). Afterwards, rock bolts can be used to reduce and control the development of fracture processes moving towards the interior. The rock bolts should pass through the region in which rock mass fractures are concentrated (slightly deeper than the EDZ). The fracture concentration area can be further extended as an extension of the EDZ (about 2 m) after the excavation of the upper layer (see Fig. 14). Therefore, in the case of the Baihetan diversion tunnel, the lengths of the rock bolts should be revised upwards, from 6 m at present to 9 m.

6. Conclusions

We have presented successful MS tests aimed at understanding the fracture processes in CJB rock masses subject to tunnel excavation. Based on the lessons learned from this exploratory investigation, the preferred MS monitoring method to use in CJB or jointed hard rock engineering has been suggested (i.e. sensor type, sensor spacing, sensor array form, system protection, and analysis region selection). The results presented here show good location accuracy and high sensitivity. They also indicate that the MS activity associated with CJB fracture is mainly induced by tunnel excavation and lasted 2–3 days during each excavation cycle in the Baihetan diversion tunnel. The area of concentration of the fractures develops at the sidewall surface and gradually moves to the interior of the surrounding rock mass during the whole process of excavation unloading. Important guidance for the further construction of the Baihetan hydropower station has been derived based on the MS results. Accordingly, the opportunity for support implementation (i.e. the support distance posterior to the tunnel face and time of concrete spraying) and support form (such as the length of the rock bolts used) have been suggested.

The support suggestions mentioned above, which were derived from these MS tests, have been adopted in the subsequent excavation of the Baihetan tunnel and powerhouse where CJB developments occur. Only a small amount of local rock instability has occurred during the construction in regions which have very adverse geological structures. Thus, the MS tests have provided effective guidance with respect to support measures as well as providing a deeper understanding of the rock mass fracturing process in CJB rock engineering.

Acknowledgments

The authors gratefully acknowledge financial support from The National Natural Science Foundation of China (Grant nos. 51509244 and 11232014). We also thank Prof. Shao-jun Li, Prof. Quan Jiang, Dr. Y. Yu, Yi-lin Fan, and Xiang-dong Zhu who helped with the microseismicity monitoring program in the diversion tunnels of the Baihetan hydropower station.

References

1 Yan DX, Xu WY, Zheng WT, Wang W, Shi AC, Wu GY. Mechanical characteristics of columnar jointed rock at dam base of Baihetan hydropower station. *J Cent South Univ*. 2001;18:2157–2162.
2 Jiang Q, Feng XT, Fan XL, Hatzor YH, Hao XJ, Li SJ. Mechanical anisotropy of columnar jointed basalts: an example from the Baihetan hydropower station, China. *Eng Geol*. 2014;175:35–45.
3 Mallet R. On the origin and mechanism of production of the prismatic (or columnar) 15 structure of basalt. *Philos Mag*. 1875;50(122–135):201–226.
4 Gilman JJ. Basalt columns, Large scale constitutional supercooling?. *J Volcanol Geotherm Res*. 2009;184:347–350.
5 Guy B, Le Coze J. Reflections on columnar jointing of basalts: the instability of the planar solidification front. *Comptes rendus De l'Académie Des Sci Paris*. 1990;311:943–949.
6 Lore J, Gao H, Aydin A. Viscoelastic thermal stress in cooling basalt flows. *J Geophys Res*. 2000;105:23695–23709.
7 Shi AC, Tang MF, Zhou QJ. Research of deformation characteristics of columnar jointed basalt at Baihetan hydropower station on Jinsha River. *Chin J Rock Mech Eng*. 2008;27:2079–2086 [in Chinese].

8 Zhao T, Fang K, Wang L, Zou J, Wei M. Estimation of elastic modulus of rock using modified point-load test. *Geotech Test J*. 2017;40:1–6.
9 Zhang W, Chen JP, Cao ZX, Wang RY. Size effect of RQD and generalized representative volume elements: a case study on an underground excavation in Baihetan dam, Southwest China. *Tunn Undergr Sp Technol*. 2013;35:89–98.
10 Cramer ML, Black MT. Design and construction of a block test in closely jointed rocks. In: *Proceedings of the 24th US Symposium on Rock Mechanics, Rock Mechanics: Theory-Experiment-Practice*; 1983:265–266.
11 Schultz RA. Limits on strength and deformation properties of jointed basaltic rock masses. *Rock Mech Rock Eng*. 1995;28:1–15.
12 Liu HN, Wang JM, Wang SJ. Experimental research of columnar jointed basalt with true triaxial apparatus at Baihetan hydropower station. *Rock Soil Mech*. 2010;31:163–171 [in Chinese].
13 Hao XJ, Feng XT, Jiang Q, Li SJ, Xiao YX. Study on unloading failure mechanism of columnar jointed rock mass in underground tunnel based on SEM experiments. *Chin J Rock Mech Eng*. 2013;32:1647–1655 [in Chinese].
14 Di SJ, Xu WY, Ning Y, Wang W, Wu G. Macro-mechanical properties of columnar jointed basaltic rock masses. *J Cent South Univ Technol*. 2011;18:2143–2149.
15 Li T, Mei TT, Sun XH, Lv YG, Sheng JQ, Cai M. A study on a water-inrush incident at Laohutai coalmine. *Int J Rock Mech Min Sci*. 2013;59:151–159.
16 Feng XT, Yu Y, Feng GL, Xiao YX, Chen BR, Jiang Q. Fractal behaviour of the microseismic energy associated with immediate rockbursts in deep, hard rock tunnels. *Tunn Undergr Sp Technol*. 2016;51:98–107.
17 Xiao YX, Feng XT, Feng GL, Liu HJ, Jiang Q, Qiu SL. Mechanism of evolution of stress–structure controlled collapse of surrounding rock in caverns: a case study from the Baihetan hydropower station in China. *Tunn Undergr Sp Technol*. 2016;51:56–67.
18 Cook NGW. The application of seismic techniques to problems in rock mechanics. *Int J Rock Mech Min Sci*. 1964;1:169–179.
19 Kaiser PK, Tannant DD, McCreath DR. Canadian Rockburst Support Handbook, Sudbury, Ontario: Geomechanics Research Centre, Laurentian University; 1996.
20 Martin CD, Read RS, Martino JB. Observation of brittle failure around a circular test tunnel. *Int J Rock Mech Min Sci*. 1997;34:1065–1073.
21 Young RP, Collins DS. Seismic studies of rock fracture at the Underground Research Laboratory, Canada. *Int J Rock Mech Min Sci*. 2001;38:787–799.
22 Xu NW, Tang CA, Li LC, et al. Microseismic monitoring and stability analysis of the left bank slope in Jinping first stage hydropower station in southwestern China. *Int J Rock Mech Min Sci*. 2011;48:950–963.
23 Luo X, Creighton A, Gough J. Passive seismic monitoring of minescale geothermal activity – a trial at Lihir mine for mine risk management. *Pure Appl Geophys*. 2010;167:119–129.
24 Xiao YX, Feng XT, Li SJ, Feng GL, Yu Y. Rock mass failure mechanisms during the evolution process of rockbursts in tunnels. *Int J Rock Mech Min Sci*. 2016;83:174–181.
25 Chen BR, Li QP, Feng XT, Xiao YX, Feng GL, Hu LX. Microseismic monitoring of columnar jointed basalt fracture activity: a trial at the Baihetan Hydropower Station, China. *J Seismol*. 2014;18:773–793.
26 Shi AC, Tang MF, Yao W. Report on Feasibility Study of Baihetan Hydropower Station (Part IV): Engineering Geology, Hangzhou: HydroChina Huadong Engineering Corporation; 2011 [in Chinese].
27 Kijko A. An algorithm for the optimum distribution of a regional seismic network-II: an analysis of the accuracy of location of local earthquakes depending on the number of seismic stations. *PAGEOPH*. 1977;115:1011–1021.
28 Hanks TC, Kanamori HA. A moment magnitude scale. *J Geophys Res*. 1979;84:2348–2350.
29 Carranza-Torres C, Fairhurst C. Application of the convergence-confinement method of tunnel design to rock masses that satisfy the Hoek-Brown failure criterion. *Tunn Undergr Sp Technol*. 2000;15:187–213.
30 Chen BR, Feng XT, Ming HJ, et al. Evolution law and mechanism of rockbursts at deep tunnels: time delayed rockburst. *Chin J Rock Mech Eng*. 2012;31:561–569 [in Chinese].
31 Feng GL, Feng XT, Chen BR, Xiao YX, Jiang Q, Li SJ. Temporal-spatial evolution characteristics of microseismic activity for columnar jointed basalt tunnel at baihetan hydropower station. *Chin J Rock Mech Eng*. 2015;34:1967–1975.
32 Xiao YX, Feng XT, Hudson JA, Chen BR, Feng GL, Liu JP. ISRM Suggested method for in situ microseismic monitoring of the fracturing process in rock masses. *Rock Mech Rock Eng*. 2016;49:343–369.
33 Feng XT. Comprehensive in Situ Observation Test and Feedback Analysis on the Failure Process of Columnar Jointed Basalt at Baihetan Hydropower Station on Jinsha River, Wuhan: Institute of Rock and Soil Mechanics, Chinese Academy of Sciences; 2013 [in Chinese].